

Robust design optimization and stochastic performance analysis of a grid-connected photovoltaic system with battery storage and hydrogen storage

Diederik Coppitters^{a,b,c,*}, Ward De Paepe^a, Francesco Contino^d

^a*Thermal Engineering and Combustion Unit, University of Mons (UMONS), Place du parc 20, 7000 Mons, Belgium*

^b*Fluid and Thermal Dynamics (FLOW), Vrije Universiteit Brussel, Pleinlaan 2, 1050 Brussels, Belgium*

^c*Combustion and Robust Optimization Group (BURN), Vrije Universiteit Brussel (VUB) and Université Libre de Bruxelles (ULB), 1050 Brussels, Belgium*

^d*Institute of Mechanics, Materials and Civil Engineering (iMMC), Université catholique de Louvain (UCLouvain), Place du Levant, 2, 1348 Louvain-la-Neuve*

Abstract

Balancing of intermittent energy such as solar energy can be achieved by batteries and hydrogen-based storage. However, combining these systems received limited attention in a grid-connected framework and its design optimization is often performed assuming fixed parameters. Hence, such optimization induces designs highly sensitive to real-world uncertainties, resulting in a drastic mismatch between simulated and actual performances. To fill the research gap on design optimization of grid-connected, hydrogen-based renewable energy systems, we performed a computationally efficient robust design optimization under different scenarios and compared the stochastic performance based on the corresponding cumulative density functions. This paper provides the optimized stochastic designs and the advantage of each design based on the financial flexibility of the system owner. The results illustrate that the economically preferred solution is a photovoltaic array, when the self-sufficiency ratio is irrelevant ($\leq 30\%$). When a higher self-sufficiency ratio threshold is of interest, i.e. up to 59%, photovoltaic-battery designs and photovoltaic-battery-hydrogen designs

*Corresponding author

Email address: diederik.coppitters@umons.ac.be (Diederik Coppitters)

provide the cost-competitive alternatives which are least-sensitive to real-world uncertainty. Conclusively, including storage systems improves the probability to attain an affordable levelized cost of electricity over the system lifetime. Future work will focus on the integration of the heat demand.

Keywords: Grid-connected demand, Hydrogen storage, Levelized Cost Of Electricity, Photovoltaic, Robust design optimization, Uncertainty Quantification.

1. Introduction

With an expected increase of 575 GW between 2018 and 2023, solar PhotoVoltaic (PV) systems dominate the renewable capacity growth [1]. Despite this expected capacity expansion, PV systems are unable to cover the entire electricity demand, due to the intermittent behavior of solar energy. To address this intermittency, the addition of an electrical energy storage system enables to store excess of solar energy and reproduce it when electricity demand exceeds PV production. For intermittent balancing, battery energy storage (from days to weeks) and hydrogen energy storage (from weeks to months) provide a flexible, adequate alternative [2]. In this framework, hydrogen energy storage is generally performed by splitting water into hydrogen and oxygen in a Proton Exchange Membrane (PEM) electrolyzer through excess electricity, because of its advantages in power density and low operating temperature [3]. The reverse reaction is performed in a PEM fuel cell to generate electricity [4].

Design optimization studies on grid-connected Hybrid Renewable Energy Systems (HRES) including battery storage and hydrogen-based storage systems configurations received attention. Parra et al. illustrated the increase in on-site energy production of a PV-powered, grid-connected dwelling by considering battery and hydrogen storage, resulting in an additional annual income of £112 and £102 respectively [5]. Pellow et al. compared battery storage and hydrogen storage for grid-connected systems and conclude that hydrogen storage

Nomenclature

A	area, m ²	δ	membrane thickness, mm
C	capacity, Ah	el	electric
CAPEX _a	annual capital expense, €	η	efficiency
E	electric energy, MWh	pl	bipolar plates
F	Faraday constant, 96 485 C/mol	σ_{mem}	membrane conductivity, S/mm
$G_{c,a}$	annual grid cost, €	act	activation
HRES	Hybrid Renewable Energy System	an	anode
I	current, A	bat	battery
LCOE	Levelized Cost Of Electricity, €/MWh	cat	cathode
N	system capacity, kW	ch	charge
OPEX _a	annual operational expense, €	con	concentration
p	pressure, Pa	dch	discharge
PEM	Proton Exchange Membrane	EL	electrolyzer
PV	PhotoVoltaic	FC	fuel cell
R	resistance, Ω	L	photogenerated
$R_{c,a}$	annual replacement costs, €	lim	limited
RDO	Robust Design Optimization	mem	membrane
SOC	State Of Charge	nom	nominal
SSR	Self Sufficiency Ratio, %	oc	open-circuit
T	temperature, K	ohm	ohmic
U	voltage, V	sh	shunt
UQ	Uncertainty Quantification	s	series
Z	compressibility factor	th	thermal
α	electrode transfer coefficient	t	tank

achieves a higher electrical Energy Stored On Invested than battery storage [6]. Zhang et al. optimized a grid-connected battery/hydrogen system, considering several operation strategies and two different cost scenarios [7]. Under the optimistic cost scenario, hydrogen storage induces a higher Net Present Value. Despite the clear advantage of this type of HRES, Eriksson et al. highlight that

incorporating hydrogen in HRES design optimization is still an anomaly (i.e. only 5 out of 30 surveyed HRES studies incorporated hydrogen-based energy systems) [8].

During model-based HRES design optimization, these studies assumed deterministic model parameters (i.e. perfectly known and free from inherent variations). However, a HRES performance is mainly characterized by parameters subject to uncertainty (e.g. stochastic nature of solar energy, operation and maintenance costs, operating temperature) [9]. Moreover, in the hydrogen market, it remains a big challenge to obtain real market values [10]. Consequently, the uncertainty on these parameters affects the HRES performance, leading to a stochastic behavior of the system objectives. Common methods that propagate parameter uncertainties through a system model and quantify the statistical moments of the objective (i.e. Uncertainty Quantification (UQ)) are surrogate model construction methods, such as Gaussian Process Regression [11] and Polynomial Chaos Expansion (PCE) [12]. During the post-process of the surrogate model (i.e. quantification of the statistical moments), PCE provides significant advantages, such as the analytic quantification of the statistical moments and the Sobol' indices out of the PCE coefficients [12].

When the mean and standard deviation of a system objective can be quantified efficiently, these statistical moments can be used as optimization objectives. Through a multi-objective optimization algorithm, a Pareto set of optimized designs can be found that makes a trade-off between minimizing the objective mean and minimizing the standard deviation (i.e. Robust Design Optimization (RDO)). The design leading to the minimum standard deviation on the objective (i.e. the robust design) is least-sensitive to the parameter uncertainties and therefore provides the most resilient performance. In surrogate-assisted RDO, the objective mean and standard deviation for every design sample are quantified via a surrogate modelling method [13, 14].

In design optimization studies of HRES, the optimal integration of battery systems and hydrogen-based energy systems in grid-connected applications received limited attention. Moreover, the model parameters are often assumed

fixed and free from inherent variations, while the rare consideration of uncertainty is limited to linear models and only a handful uncertain parameters (<5), characterized by generic ranges based on expert judgement and assumptions [15–18]. Akbari et al. evaluated a distributed energy system, subject to a general variability of $\pm 20\%$ for a handful of financial parameters and demand parameters [17]. Parisio et al. considered the converter efficiencies related to electricity and heat demand to be uncertain between a general range of $\pm 10\%$ on a linear model of an energy hub [18]. These linear models are subject to large inherent uncertainty, while the variation of other highly-uncertain parameters (e.g. investment cost, lifetime) during real-world design, planning and operation is ignored. Moreover, generic variability ranges assume equal weights for every uncertainty, which leads to biased results. Combined, these assumptions bring forward designs that are highly sensitive to real-world uncertainties and result in a drastic mismatch between simulated and actual performances. To fill the research gap on design optimization of grid-connected, hydrogen-based HRES design optimization under uncertainty, we provide the following three novelties: All significant techno-economic uncertain parameters are characterized by their uncertainty described in literature; the uncertainties are propagated through a computationally-efficient sparse PCE algorithm, which provides the sensitivity indices without additional computational cost and unlocks a computationally-efficient RDO method subject to a large stochastic dimension; the Cumulative Density Function (CDF) of the optimized designs is used to determine the advantage of each design, based on the financial flexibility of the system owner.

In this paper, the HRES model and the RDO method are described in section 2. The optimized designs for every demand type and their stochastic performance are presented in section 3. Conclusively, section 4 illustrates the main conclusions of this work, while the appendix consists of the detailed dataset and convergence curves of the sparse PCE method.

2. Method

In the first part of this section, the HRES is introduced, followed by the Python-based component models, the climate data and the load profiles. To determine the optimized designs of the HRES, the second part of this section illustrates the uncertainty characterization and the RDO algorithm.

2.1. Hybrid Renewable Energy System

The considered system is a grid-connected load, supported by a HRES (Figure 1). The HRES consists of a PV array, which is coupled to a DC bus bar through a DC-DC converter with Maximum Power Point Tracking. A battery stack and electrolyzer array with storage tank are integrated to store the excess of PV array electricity. A fuel cell array is implemented to produce electricity from the stored hydrogen. To transfer the DC electricity from the battery system and fuel cell to the AC load, a DC-AC converter is connected.

To set the hierarchy between the subsystems, a typical power management strategy is implemented, which primarily aims to satisfy the demand [19]. In this strategy, excess PV power (i.e. remaining PV power after complying with the power required by the load) is supplied to the battery stack. When the determined charge current violates the maximum charge current, the nominal charge current is considered instead. Then, or when the battery array reaches its maximum State Of Charge (SOC), the surplus energy is used to power the electrolyzer array. When the hydrogen tank is full, or when the surplus power lies outside the electrolyzer array operating range, the surplus energy is sold to the grid at the wholesale electricity price [20].

In the opposite case, when the PV array does not cover the demand, the remaining demand is covered by the battery array, if the discharge current does not violate the maximum discharge current and the SOC remains above the SOC lower limit. If not, nominal discharge current is extracted and the additional power is supplied by the fuel cell array. When insufficient, the grid covers the remaining demand.

In the following subsections, the PV, battery, electrolyzer, fuel cell, storage tank, DC-DC converter and DC-AC inverter component models are described. The final subsection illustrates the characterization of the climate profiles and demand profiles.

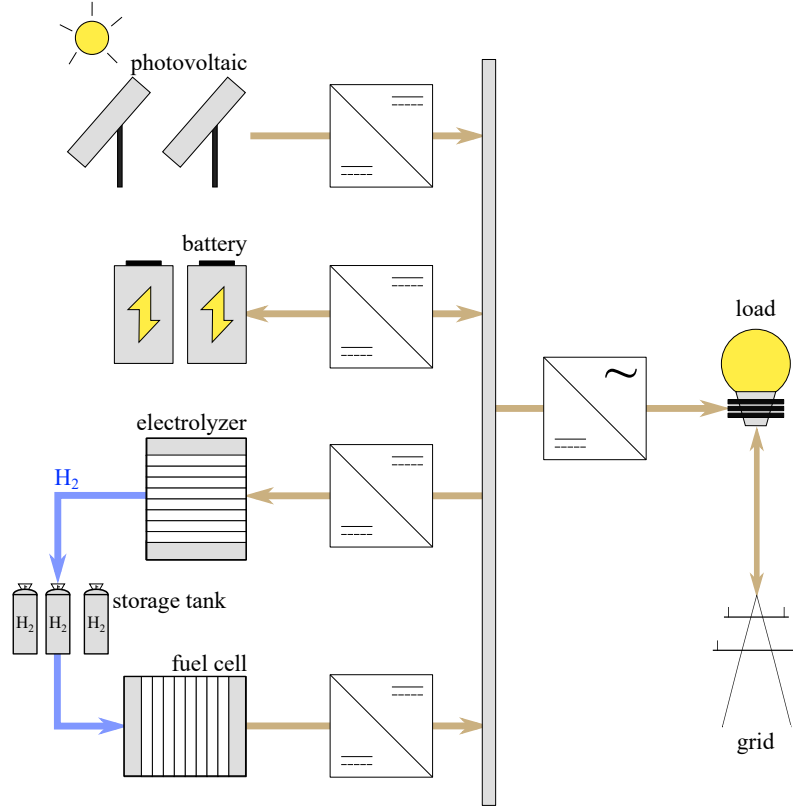


Figure 1: The considered system includes the load connected to the grid and supported by a Hybrid Renewable Energy System (HRES). This HRES consists of a PhotoVoltaic (PV) array which converts solar energy into electricity. The battery stack and hydrogen-based energy system (electrolyzer, fuel cell and storage tank) enable the system to store excess of PV array electricity and to comply, up to the available energy, with the demand when the solar irradiance is insufficient.

2.1.1. Photovoltaic array

To determine the electricity produced by a PV array, we imported the experimentally-validated model out of the PVlib Python library [21, 22]. The

model quantifies the PV panel current-voltage characteristic through the following single-diode equation:

$$I_{PV} = I_L - I_0 \left(\exp \left(\frac{U + IR_s}{n_{diode} N_s U_{th}} \right) - 1 \right) - \frac{U + IR_s}{R_{sh}}. \quad (1)$$

The parameters in Equation 1 are not provided by the PV manufacturer. Therefore, we adopted the method by De Soto et al. to determine these parameters out of manufacturer data [23, 24].

2.1.2. Battery stack

A lead-acid battery technology is selected in this work, as it is the most widespread technology and a mature lead-acid battery industry exists with significant learning rates during the last decades [25]. Despite the higher power and energy density of lithium-based electrochemical batteries and the significant market share in the future, currently the installation experience and availability is limited [25], and the uncertainty on the cost is still large as opposed to lead-acid batteries [26]. To characterize the performance of a lead-acid battery stack, we adopted the experimentally-validated model of Blaifi et al. [27]. The general voltage-current relation for a lead-acid battery is defined as:

$$U_{bat} = U_{bat,oc} + I_{bat} R_{bat}, \quad (2)$$

where the current I_{bat} is positive during charge and negative during discharge. The resistance component R_{bat} is different during charge and discharge and depends on the temperature, the current magnitude and the capacity. Therefore, the characterization of the voltage during charge and discharge is given by:

$$U_{ch} = (2.085 - 0.12(1 - SOC)) - \frac{I}{C_{nom}} \left(\frac{4}{1 + I^{1.3}} + \frac{0.27}{SOC^{1.5}} + 0.02 \right) (1 - 0.007\Delta T), \quad (3)$$

$$U_{dch} = (2 - 0.16 SOC) + \frac{I}{C_{nom}} \left(\frac{6}{1 + I^{0.86}} + \frac{0.48}{(1 - SOC)^{1.2}} + 0.036 \right) (1 - 0.025\Delta T). \quad (4)$$

The State Of Charge (SOC) is the fraction of the total capacity stored in the battery:

$$\text{SOC}(t) = \text{SOC}_0 + \frac{1}{C(t)} \int_0^t \eta_{\text{bat}}(t) I(t) dt, \quad (5)$$

In this work, the minimum SOC is set at 20% [26, 28].

The battery stack lifetime is characterized by the Depth Of Discharge ($= 1 - \text{SOC}$), the charge current, discharge current and operating time in the overcharge zone and overdischarge zone. We estimated the lifetime based on SOC variations through the commonly implemented Rainflow cycles counting method [29]. To avoid excessive reduction of the lifetime and active mass losses due to gassing effects, overcharging and overdischarging are avoided, while the maximum charge current and maximum discharge current are limited to $C_{\text{nom}}/10$ and $C_{\text{nom}}/3.3$, respectively [30]. Because of the constraints limiting the operation in the optimal operating zone to prolong battery life, we assumed a yearly capacity degradation rate [31] and a fixed energy efficiency of 80% [32].

2.1.3. Electrolyzer array

We selected a Proton Exchange Membrane (PEM) electrolyzer for its fast response time (<1 s) and full load flexibility (0% - 100%) [33]. Despite the effect of intermittent loading on degradation and lifetime is not yet well quantified, this effect is reported to be negligible by several manufacturers [33]. Therefore, this effect is not considered in this study and a fixed degradation rate per operating hour is assumed. To evaluate this procedure and to determine the voltage-current characteristic, efficiency and hydrogen flow rate, we selected the experimentally-validated model from Abdin et al. and we consider an operating pressure of 30 bar [34, 35]. The operating voltage is characterized according to the following equation:

$$U_{\text{EL}} = U_{\text{EL,oc}} - U_{\text{EL,act}} - U_{\text{EL,ohm}} - U_{\text{EL,con}}. \quad (6)$$

In the remainder of this subsection, the subscript "EL", which refers to electrolyzer, is left out for ease of reading. The open-circuit voltage follows out of

the Nernst equation for electrolysis:

$$U_{oc} = (1.229 - 0.9 \times 10^{-3} (T - 298)) + \frac{R_u T}{2F} \left(\ln \left(\frac{p_{H_2} \sqrt{p_{O_2}}}{a_{H_2O}} \right) \right), \quad (7)$$

where R_u , F and a represent the universal gas constant, Faraday constant and water activity between electrode and membrane, respectively. The activation overpotential U_{act} represents the voltage used to transfer electrons between the electrodes. By inverting the Butler-Volmer equation for the reactions at the electrode surface, the activation voltage can be quantified:

$$U_{act} = \frac{R_u T}{\alpha_{an} F} \operatorname{arcsinh} \left(\frac{i}{2i_{0,an}} \right) + \frac{R_u T}{\alpha_{cat} F} \operatorname{arcsinh} \left(\frac{i}{2i_{0,cat}} \right), \quad (8)$$

where values from experimental work are selected to quantify the electrode transfer coefficients and exchange current densities [34]. At high currents, a concentration overpotential U_{con} is created due to an excess of reactants (e.g. oxygen bubbles slowing down the reaction). To quantify this overpotential, a combination of the Nernst equation and Fick's law is adopted:

$$U_{con} = \frac{R_u T}{4F} \ln \frac{C_{O_2}^{mem}}{C_{O_2,0}^{mem}} + \frac{R_u T}{2F} \ln \frac{C_{H_2}^{mem}}{C_{H_2,0}^{mem}}, \quad (9)$$

where C^{mem} is the concentration at the membrane-electrode interface, and the subscript 0 refers to the reference working condition. The final overpotential that occurs in the PEM electrolyzer is the ohmic overpotential U_{ohm} , which is driven by the electric resistance of the electrodes R_{el} , bipolar plates R_{pl} and the membrane R_{mem} :

$$U_{ohm} = I (R_{el} + R_{pl} + R_{mem}). \quad (10)$$

The electric resistance of the electrodes and the flow plates can be quantified by applying Ohms law. We refer to Abdin et al. for further details on the determination of the overpotentials [34]. Finally, following the working point of the electrolyzer array, the hydrogen molar flow rate \bar{n}_{H_2} is formulated as:

$$\bar{n}_{H_2} = \frac{I}{2F}. \quad (11)$$

2.1.4. Hydrogen storage tank

The pressurized hydrogen produced in the electrolyzer is stored in a storage tank. Filling up the storage tank increases the tank pressure, until the electrolyzer outlet pressure is reached, according to the ideal gas law [36]:

$$p_t - p_{t,\text{init}} = Z \frac{N_{\text{H}_2} R_u T_t}{M_{\text{H}_2} V_t}. \quad (12)$$

The compressibility factor Z for H_2 is equal to 1 at room temperature and moderate pressure (<100 bar) [36].

2.1.5. Fuel cell array

To generate electricity by converting hydrogen and oxygen into water, we selected a PEM fuel cell. The PEM fuel cell is a widespread commercial technology, which operates at low operational temperature (70 °C- 100 °C) and achieves high power densities (up to 2 W/cm²). Similar to the PEM electrolyzer, the effect of intermittent operation on the degradation and lifetime is not yet fully understood [37]. Therefore, a fixed degradation rate per operating hour is assumed. To represent this conversion of hydrogen and oxygen into water, we adopted the model from Murugesan et al. which is experimentally validated on the Ballard-Mark-V PEM fuel cell [38].

To determine the electric power production, the operating current and voltage are required. The operating current depends on the converted hydrogen molar flow rate:

$$I_{\text{FC}} = 2F n_{\text{FC},\text{H}_2}. \quad (13)$$

The electric potential produced during water composition out of hydrogen and oxygen is equal to the Nernst potential minus the losses:

$$U_{\text{FC}} = U_{\text{FC},\text{Nernst}} - U_{\text{FC},\text{act}} - U_{\text{FC},\text{ohm}} - U_{\text{FC},\text{con}}. \quad (14)$$

In the remainder of this subsection, the subscript FC is again left out for ease of reading. The Nernst equation determines the maximum fuel cell voltage and

considers the operating temperature and reactant pressures:

$$U_{\text{Nernst}} = 1.229 - 0.85 \times 10^{-3}(T - 298.15) + 4.31 \times 10^{-5}T (\ln(p_{\text{H}_2}) + 0.5 \ln(p_{\text{O}_2})). \quad (15)$$

The activation losses U_{act} occur due to a low rate of charge transfer at lower current densities. This activation loss corresponds to:

$$U_{\text{act}} = -0.948 + 0.00354T + 7.6 \times 10^{-5}T \ln(C_{\text{O}_2}) + -1.93 \times 10^{-4}T \ln(I). \quad (16)$$

The ohmic losses U_{ohm} occur out of electrolyte resistance, contact resistance at the collector plates and at the graphite electrodes. This loss is linearly dependent to the load:

$$U_{\text{ohm}} = iR_{\text{ohm}} = i \frac{\delta_{\text{mem}}}{\sigma_{\text{mem}}}, \quad (17)$$

where R_{ohm} is the electrical resistance that depends on the membrane thickness δ_{mem} and membrane conductivity σ_{mem} (Nafion 117). The concentration loss occurs due to changes in concentration of reactants at higher current density region:

$$U_{\text{con}} = -0.016 \ln \left(1 - \frac{i}{i_{\text{lim}}} \right). \quad (18)$$

We refer to the work of Murugesan et al. for the detailed quantification of these losses [38].

2.1.6. Power conversion

The components are connected to a DC bus bar through DC-DC converters. To provide the power to the load or the grid, the DC bus bar is connected through a DC-AC inverter. The conversion efficiency of a DC-DC converter η_{conv} depends on the component output power:

$$P_{\text{DC,out}} = \eta_{\text{conv}} (P_{\text{DC,out}}) P_{\text{DC,in}}. \quad (19)$$

The conversion efficiency depends on the converter type. We considered the experimentally buck-boost converter efficiency profile presented by Taghvaei et al. for the PV array, PEM electrolyzer array and fuel cell array and a bidirectional buck-boost converter efficiency profile for the battery stack [39]. Similar to the

DC-DC converter, the DC-AC inverter efficiency profile η_{inv} depends on the AC output power $P_{\text{AC,out}}$:

$$P_{\text{AC,out}} = \eta_{\text{inv}}(P_{\text{AC,out}}) P_{\text{DC,in}}. \quad (20)$$

In this work, the inverter efficiency profile is determined by the experimentally-validated method described by Rampinelli et al. [40].

2.1.7. Climate and demand data

The HRES performance depends on the climate and demand characteristics. In this work, we evaluated a dwelling and a community (i.e. 2500 dwellings) in Brussels (Belgium). When adopting climate data and demand data, it is important to adopt the climate data that was used to generate the demand data, as the solar irradiance and ambient temperature affect how the demand behaves. Therefore, we appeal to Typical Meteorological Year data and hourly demand data from the National Renewable Energy Laboratory, as the former is used to construct the latter [41, 42]. As the data only exists for locations in the United States of America, we applied the method presented by Montero Carrero et al. to adapt the climate and demand profiles for Belgium [43] (Figure 2).

2.2. Robust Design Optimization

This section introduces the design parameters of the HRES are introduces, as well as the objective and indicator to characterize the performance of each design. Additionally, this section also provides the uncertainty characterization of the model parameters, followed by the UQ technique to propagate these uncertainties through the model and by the optimization algorithm.

2.2.1. Design parameters, objective and indicator

The capacity of the PV array, battery stack, PEM electrolyzer array, PEM fuel cell array and storage tank are selected as continuous design parameters. By considering the capacities as independent design parameters, the optimization algorithm is able to exclude any technology from the HRES. Selecting large system capacities enables to cover a significant part of the demand with the HRES,

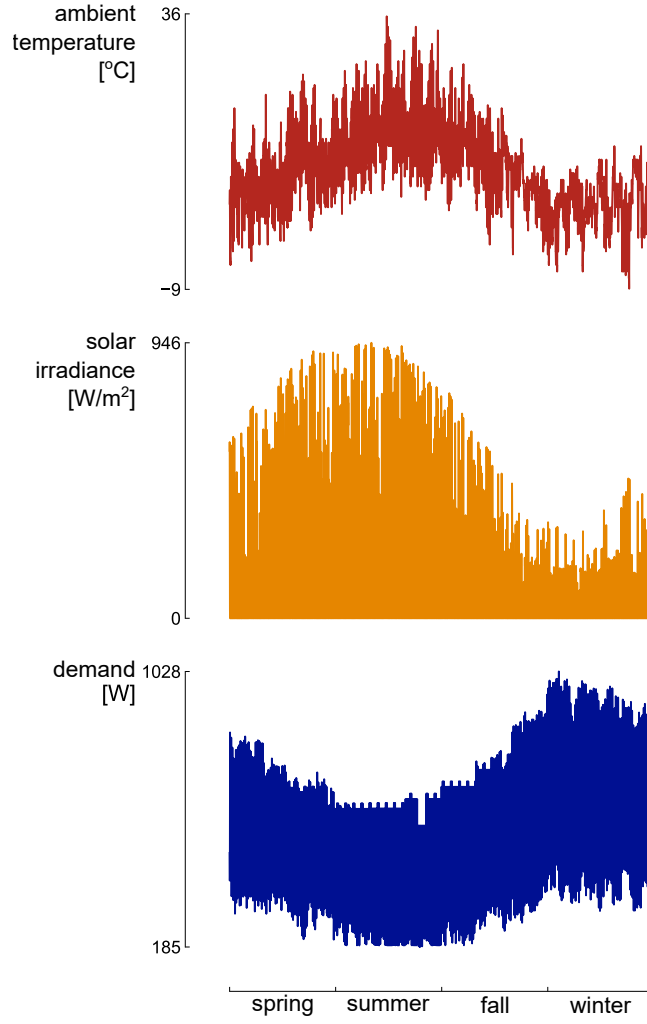


Figure 2: The climate data (solar irradiance and ambient temperature) and demand data are inversely proportional, resulting in a reduced demand during spring and summer and a peak demand during fall and winter.

but induces large investment, operating and replacement costs. To evaluate the techno-economic performance of the HRES designs, minimizing the Levelized Cost Of Electricity (LCOE) is defined as the system objective. The LCOE of the hybrid system reflects the system cost per unit of electricity covered [28]:

$$\text{LCOE} = \frac{\text{CAPEX}_a + \text{OPEX}_a + R_{c,a} + G_{c,a} - G_{s,a}}{\sum_{i=0}^{8760} P_{\text{load}}}. \quad (21)$$

To determine the system cost, the annualized investment cost CAPEX_a , operational cost OPEX_a , replacement cost $R_{c,a}$, grid electricity cost $G_{c,a}$ and the gain from selling excess electricity $G_{s,a}$ are evaluated. We refer to Zakeri et al. for the detailed quantification of these parameters [28]. The specific cost parameters values are listed in Table A.3.

To indicate the fraction of the load that is covered by the HRES, the Self-Sufficiency Ratio (SSR) is quantified as an indicator for the HRES performance [7]:

$$\text{SSR} = 1 - \frac{E_{\text{grid}}}{E_{\text{load}}}, \quad (22)$$

where E_{load} is the total energy demand over the system lifetime. The SSR is an important factor for adopters of HRES, as it illustrates the resilience against large electricity price increases and the protection against power cuts, which are more likely in the future [44]. Moreover, reaching a significant SSR threshold is beneficial for grid operators, as it reduces the simultaneous power extraction from the grid and therefore reduces the risk of black-outs.

2.2.2. Uncertainty characterization and quantification

To represent the uncertainty during design and operation of the HRES, the model parameters are characterized by a uniform distribution based on literature (Table A.3). During operation, the system is subject to natural variability of the technical parameters, e.g. fluctuating operating temperature and pressure, varying degradation speed and an uncertain component lifetime. Additionally, inter-annual variability is present on the electricity demand, solar irradiance and ambient temperature [9]. From an economic point of view, the system is subject to commissioning and maintenance quality, which affects the operating and maintenance cost, an uncertain replacement cost due to evolving market conditions and a highly-uncertain wholesale electricity price due to an evolving energy mix, improved energy efficiency and increased electrification of fossil-based energy sectors [45]. The interest rate and the investment cost can be considered deterministic or uncertain, depending on the actual step of the design process and the finance type considered [9]. Most studies assume a single-stage

investment at the project start, which implies a deterministic characterization of these parameters. However, a change in the finance type of the project and a significant timeframe between the design stage and investment stage, which increases the possibility for the market conditions to change between the stages, implies uncertainty on the interest rate and investment costs. Therefore, in this work, two scenarios are assumed. The first scenario considers the interest rate and investment costs as deterministic (i.e. fixed market conditions), while the second scenario treats these parameters as uncertain (i.e. varying market conditions). As the results are significantly influenced by the design step and investment type, the handling of two scenarios enables to compare with both commonly adopted scenarios in scientific literature.

The uncertainty on the input model parameters propagates through the model, inducing variability on the performance indicators of the HRES. Following the computational cost of the model evaluation (≈ 150 s) and the large number of uncertainties considered (36 in the variable market conditions scenario and 28 in the fixed market conditions scenario), we considered a computationally efficient sparse Polynomial Chaos Expansion (PCE) method to propagate the uncertainty and quantify the statistical moments of the model output [46]. The method deals with the computational intractability when a large stochastic dimension (> 10) is considered in state-of-the-art methods, such as Monte Carlo Simulation and full PCE. Next to these statistical moments, the contribution of each stochastic parameter to the variance of the objective provides valuable information on the system behavior under uncertainty. Generally, this contribution is quantified through Sobol' indices. PCE provides an analytical solution to quantify these Sobol' indices through post-processing of the coefficients (i.e. no additional model evaluations required). Additional details of this sparse PCE method are described by Abraham et al. [46]. In this work, a polynomial order of 3 is required to approximate the real model behavior accurately ($< 1\%$ error on the statistical moments, compared to a Monte Carlo Simulation result). The sparse PCE method achieves a similar accuracy with only 29% of the required evaluations for PCE (Figure A.9), leading to a significant increase

in computational efficiency of the method.

2.2.3. Robust design optimization

During system design, several design parameters have to be quantified such that they simultaneously lead to the optimal system performance. For this system, the system performance is determined by the mean and standard deviation of the LCOE. While minimizing the LCOE mean is beneficial for the average expected cost of electricity paid by the system owner, reducing the LCOE standard deviation increases the probability of operating near that LCOE mean in reality. For every evaluated design, the sparse PCE method is applied to quantify the statistical moments. The sparse PCE method is coupled to the Nondominated Sorting Genetic Algorithm (NSGA-II) to find the set of design that make a trade-off between minimizing the mean and standard deviation of the LCOE [47, 48]. In this work, the population size is fixed at 50 design samples (i.e. based on a rule of thumb of 10 samples per design parameter [49]). The optimization algorithm is characterized with a crossover and mutation probability of 0.9 and 0.1 respectively.

3. Results and discussion

The UQ and RDO method are applied to the HRES to determine the optimized designs and to evaluate their performance under the variable market conditions scenario and fixed market conditions scenario. First, the Pareto set of optimized designs is presented, supplemented by a global sensitivity analysis to capture the driving uncertainties. Additionally, the stochastic design performance of these optimized designs is compared based on the Cumulative Distribution Function (CDF).

3.1. Robust Design Optimization and global sensitivity analysis

The RDO method is applied four times independently on the HRES: for the dwelling and community in the fixed market conditions scenario and the variable market conditions scenario. In both scenarios, a trade-off exists between

minimizing the LCOE mean and minimizing the LCOE standard deviation for the dwelling (Figure 3) and for the community (Figure 4), which is illustrated by the Pareto set of optimized designs. For each optimized design, the total Sobol' indices of the LCOE and the statistical moments of the corresponding SSR are quantified.

The minimum LCOE mean is achieved by a PV array (e.g. 2.7 kW_p for the dwelling), which in the variable market conditions scenario induces a slightly larger LCOE standard deviation (e.g. 55.9 €/MWh for the dwelling) than in the fixed market conditions scenario (e.g. 55.1 €/MWh for the dwelling), due to the additional uncertainty present on the PV array investment cost and interest rate (Figure 3 and Figure 4). For this design, the uncertainty related to the grid electricity price (i.e. wholesale electricity price and proportion of the wholesale electricity price in the total charged cost per MWh consumed) dominates the LCOE standard deviation, due to the significant dependency on the grid to comply with the electricity demand (SSR mean = 30%). To reduce the LCOE standard deviation, at the expense of a minimal increase in LCOE mean, the Pareto set of optimized designs implies to increase the PV array capacity, which consequently increases the SSR mean and therefore decreases the Sobol' indices related to grid electricity. To illustrate for the dwelling, increasing the PV array capacity proves to be a cost-efficient approach (i.e. with minimal increase in LCOE mean) to decrease the LCOE standard deviation down to 48.5 €/MWh in the variable market conditions scenario and down to 42.6 €/MWh in the fixed market conditions scenario. Despite the LCOE standard deviation can be reduced modestly by increasing the PV array capacity, the proposed PV designs remain primarily dependent on grid electricity (SSR mean < 40%) and the envisioned LCOE is therefore subject to a significant standard deviation.

To further decrease the LCOE standard deviation over a higher SSR mean threshold (e.g. SSR mean > 40% for the community, Figure 4), PV-battery designs are configured by the optimization algorithm, instead of further increasing solely the PV array capacity. This because the SSR mean stagnates over a certain PV capacity threshold, while the inclusion of a battery stack enables to

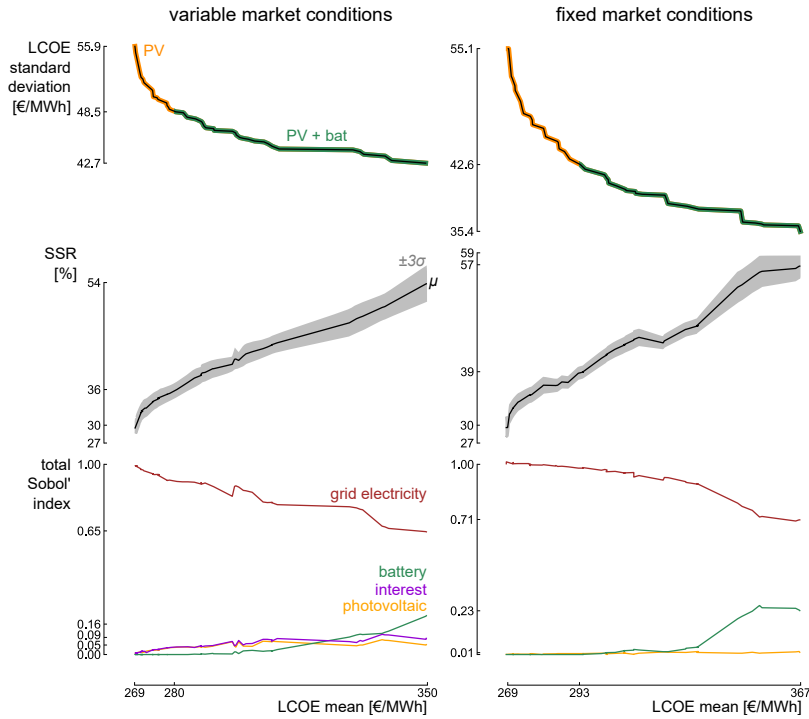


Figure 3: For the dwelling, the Pareto front illustrates that a trade-off exists between minimizing the Levelized Cost Of Electricity (LCOE) mean and LCOE standard deviation. Reducing the LCOE standard deviation cost-efficiently is suggested by subsequently expanding a PV array and battery stack. This system capacity evolution improves the mean Self-Sufficiency Ratio (SSR) and consequently reduces the importance of the grid price uncertainty. Instead, the uncertainty related to the interest rate (in the variable market conditions scenario) and the battery stack gradually gain in importance in the LCOE variation.

cover part of the demand when insufficient solar irradiance is available. Hence, the optimization algorithm suggests designs which subsequently increase in both PV array capacity and battery stack capacity to further reduce the LCOE standard deviation (and thus increase in SSR mean). For these designs, the LCOE standard deviation is significantly characterized by the uncertainty related to the battery (e.g. total Sobol' index up to 16% in the variable market conditions scenario for the dwelling, Figure 3). Therefore, improving the battery lifetime estimation is considered an effective approach to reduce the LCOE standard deviation of these designs with an external measure.

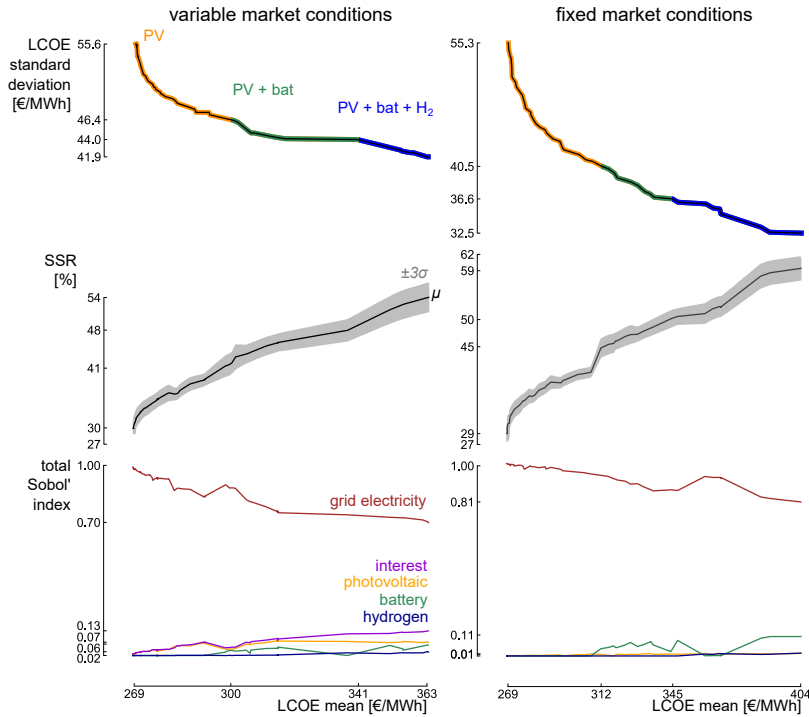


Figure 4: For the community, the Pareto front illustrates that a trade-off exists between minimizing the Levelized Cost Of Electricity (LCOE) mean and LCOE standard deviation. Reducing the LCOE standard deviation cost-efficiently is suggested by subsequently expanding a PV array, battery stack and the hydrogen-based energy system. This system capacity evolution improves the mean Self-Sufficiency Ratio (SSR) and consequently reduces the importance of the grid price uncertainty. Instead, the uncertainty related to the interest rate (in the variable market conditions scenario) and the battery stack gradually gain in importance in the LCOE variation.

For the dwelling, a PV-battery configuration defines the robust design which achieves an SSR mean of 54% in the variable market conditions scenario and an SSR mean of 57% in the fixed market conditions scenario. Consequently, from this point, improving the SSR mean leads to an increase in LCOE standard deviation due to the significant increase in system capacity, from which the corresponding uncertainty overcompensates the reduction in the uncertainty related to grid electricity. As lower uncertainty is related to the system capacity in the fixed market conditions scenario (i.e. deterministic investment costs), the

SSR mean for the robust design in this scenario is higher than for the robust design in the variable market scenario. Therefore, the LCOE standard deviation for the robust design in the fixed market conditions scenario (35.4€/MWh) is lower than for the robust design characterized in the variable market scenario (42.7€/MWh). For the community, the robust design includes both a battery stack and a hydrogen-based energy system (Figure 4), despite the large uncertainty related to the specific cost of the electrolyzer and fuel cell (e.g. $\sigma_{\text{CAPEX}_{\text{EL}}} = 202 \text{ €/kW}$ as opposed to $\sigma_{\text{CAPEX}_{\text{bat}}} = 73 \text{ €/kWh}$). The decoupling of power (i.e. electrolyzer and fuel cell) and energy (i.e. hydrogen tank, $\sigma_{\text{CAPEX}_{\text{tank}}} = 1.2 \text{ €/kWh}$) enables to curb the uncertainty related to the hydrogen-based energy system present in the LCOE standard deviation. Moreover, this decoupling enables to provide a cost-efficient alternative for a large battery stack at moderate SSR. Therefore, a PV-battery-hydrogen design is configured as a robust alternative in both scenarios for the community.

Table 1: The characteristics of the three evaluated optimized designs for the dwelling: a PV design and a PV-battery design that achieve the lowest LCOE mean among their corresponding category and the PV-battery robust design that achieves the lowest LCOE standard deviation.

	N_{PV}	N_{Bat}	μ_{LCOE}	σ_{LCOE}	μ_{SSR}
	kW _p	kWh	€/MWh	€/MWh	%
variable market scenario					
PV	2.7		269	55.9	30
PV + bat	5.1	1.0	280	48.5	36
PV + bat robust	5.2	6.9	350	42.7	54
fixed market scenario					
PV	2.7		269	55.1	30
PV + bat	6.9	1.1	293	42.6	39
PV + bat robust	9.1	5.8	367	35.4	57

Table 2: The characteristics of the three evaluated optimized designs for the community: a PV design and a PV-battery design that achieve the lowest LCOE mean among their corresponding category and the PV-battery-hydrogen robust design that achieves the lowest LCOE standard deviation.

	N_{PV}	N_{Bat}	N_{ELEC}	N_{FC}	N_{tank}	μ_{LCOE}	σ_{LCOE}	μ_{SSR}
	MW _p	MWh	MW	MW	MWh	€/MWh	€/MWh	%
variable market scenario								
PV	6.9					269	55.6	30
PV + bat	11.6	6.1				300	46.4	41
PV + bat + H ₂	16.3	7.1	1.7	0.5	16.7	363	41.9	54
fixed market scenario								
PV	6.5					269	55.3	29
PV + bat	15.0	6.9				312	40.5	45
PV + bat + H ₂	21.2	8.4	2.3	0.5	16.7	404	32.5	59

3.2. Comparison of stochastic performance

Due to the trade-off between minimizing the LCOE mean and minimizing the LCOE standard deviation, each design out of the Pareto set of optimized designs carries an advantage in either average performance or robustness. To evaluate the overall stochastic performance, the CDF is constructed for three representative optimized designs: the PV design that achieves the lowest LCOE mean, the PV-battery design that achieves the lowest LCOE mean among the proposed PV-battery designs and a robust design, which corresponds to the lowest LCOE standard deviation for the dwelling (Table 1) and for the community (Table 2). Among these designs, the PV design achieves the highest probability that in reality, the resulting LCOE over the lifetime will be lower than any predefined LCOE upper limit for the dwelling and community (yellow CDF on Figure 5 and Figure 6, respectively). To illustrate in a variable market conditions scenario, if the dwelling owner predefines an LCOE upper limit of 250 €/MWh to ensure an affordable cost of electricity, the PV design provides a probability of 44 % that the LCOE in reality will be below or equal to that upper limit. Alternatively, a lower probability that the real LCOE will be below this upper limit is achieved by the PV-battery design (33 %) and by full grid-dependency (24 %). However,

when the upper limit value is determined higher or equal to 350 €/MWh in the variable market conditions scenario (374 €/MWh in the fixed market conditions scenario), the PV-battery design achieves a similar probability to result in an LCOE below the upper limit as the PV design. This observation is explained by the lower LCOE standard deviation of the PV-battery design, which steepens the corresponding CDF and therefore realises the intersection between the PV and PV-battery CDF, despite the larger LCOE mean of the PV-battery design.

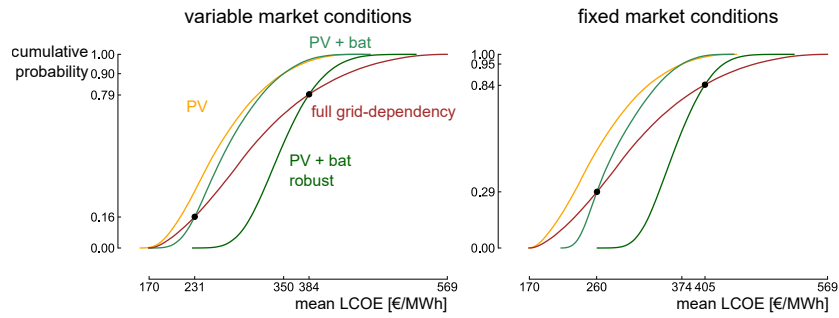


Figure 5: The Cumulative Density Functions (CDF) of three optimized designs and full grid-dependency for the dwelling. The intersection point between two CDFs illustrates the minimum LCOE upper limit that has to be defined, in order for the optimized design to achieve a higher probability than full grid-dependency to achieve an LCOE below this upper limit in reality.

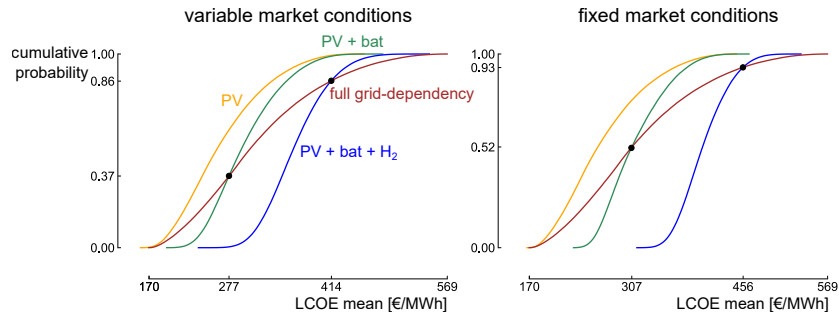


Figure 6: The Cumulative Density Functions (CDF) of three optimized designs and full grid-dependency for the community. The intersection point between two CDFs illustrates the minimum LCOE upper limit that has to be defined, in order for the optimized design to achieve a higher probability than full grid-dependency to achieve an LCOE below this upper limit in reality.

The PV design achieves a rather low SSR mean (30%), which makes this design vulnerable to grid behavior, fluctuating electricity prices and potential power cuts. Moreover, operating over a higher SSR threshold reduces the risk of black-out, as it avoids the simultaneous power extraction from the grid of different demand types. Therefore, the PV-battery design and robust design are of interest when operating over a larger SSR threshold is preferred (Figure 7 for the dwelling and Figure 8 for the community). To illustrate for the dwelling in a variable market scenario, the PV-battery design with the lowest LCOE mean achieves an SSR mean of 36%, while the robust PV-battery design achieves an SSR mean of 54%.

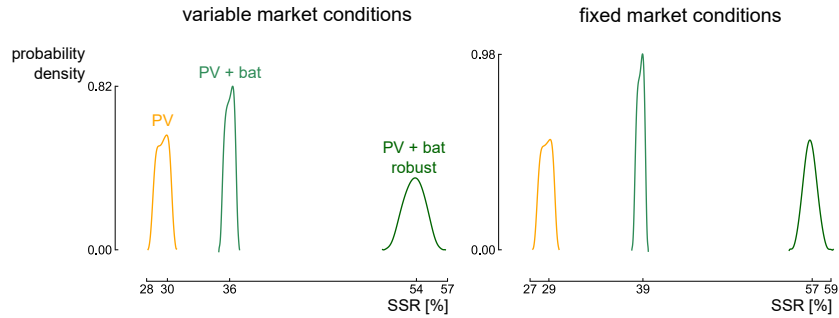


Figure 7: For the dwelling, the probability density functions of the SSR for three optimized designs illustrate the different SSR thresholds over which the designs operate.

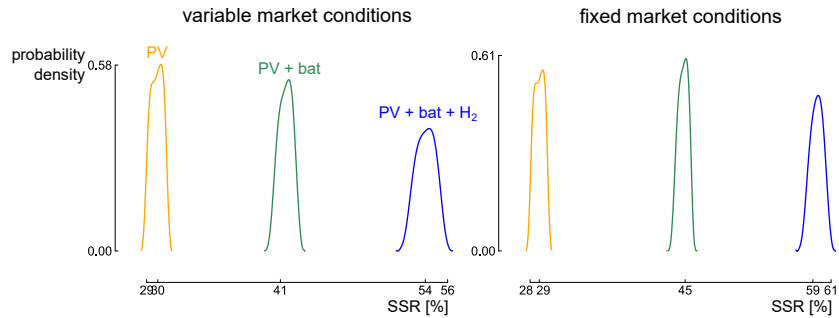


Figure 8: For the community, the probability density functions of the SSR for three optimized designs illustrate the different SSR thresholds over which the designs operate.

When operating over a higher SSR threshold is considered, the performance of the PV-battery design (green CDF on Figure 5 and Figure 6) is of interest and

can be compared with full grid-dependency (red CDF on Figure 5 and Figure 6). In this comparison, the preferred design depends on the predefined LCOE upper limit (and thus on the financial flexibility of the owner). To illustrate for the dwelling in the variable market conditions scenario, both the PV-battery design and full grid-dependency result in a probability of 16 % that the LCOE in reality will be below or equal to 231 €/MWh. If the LCOE upper limit is estimated even lower by the building owner to ensure an affordable cost of electricity, full grid-dependency results in a higher probability to end up below the upper limit than the PV-battery design: e.g. full grid-dependency achieves a probability of 6 % that the LCOE in reality will be below 200 €/MWh, while the PV-battery design ensures a probability of only 1 %. Instead, if the LCOE upper limit is set higher than 231 €/MWh, the PV-battery design ensures a higher probability: e.g. full grid-dependency results in a probability of 49 % that the LCOE in reality will be below or equal to 300 €/MWh, while the PV-battery design ensures a probability of 68 %. Conclusively, when the household projects an LCOE of at least 231 €/MWh as a maximum to ensure an affordable cost of electricity, the PV-battery design provides a higher probability to comply with this upper limit than full grid-dependency. Similar results are presented for the community.

Despite the lowest LCOE standard deviation, the CDF of the robust designs do not intersect with the other evaluated optimized designs and is therefore only of interest when operating over a larger SSR threshold. If so, then the robust PV-battery design for the dwelling (darkgreen CDF on Figure 5) proves to be beneficial over full grid-dependency when the LCOE upper limit is set above 384 €/MWh in the variable market conditions scenario and above 405 €/MWh in the fixed market conditions scenario. For the community, a PV-battery-hydrogen configuration is characterized as a robust design (blue CDF on Figure 6). This design is beneficial over full grid-dependency when the LCOE upper limit is defined higher than 414 €/MWh in the variable market conditions scenario and higher than 456 €/MWh in the the fixed market conditions scenario. Consequently, a PV-battery-hydrogen design presents a cost-competitive alternative over full grid-dependency and moreover operates over a significant

SSR threshold ($\geq 54\%$), which reduces the risk of black-out and power cuts.

4. Conclusion

The robust design optimization method illustrates a trade-off between minimizing the levelized cost of electricity mean and minimizing the standard deviation for a dwelling and a community. A photovoltaic array achieves the lowest levelized cost of electricity mean (i.e. 269 €/MWh). Additionally, such a system ensures the highest probability that the levelized cost of electricity in reality will be below an upper limit, which has been predicted by the system owner to ensure an affordable cost of electricity. Nevertheless, the proposed photovoltaic arrays remain primarily dependent on grid electricity (self – sufficiency ratio mean $\approx 30\%$) and therefore subject to a significant standard deviation, risk of black-out and power cuts.

Photovoltaic-battery designs reduce this grid-dependency by increasing the self-sufficiency ratio and therefore decrease the levelized cost of electricity standard deviation. When operating over a higher self-sufficiency ratio is of interest, these photovoltaic-battery design are able to ensure a higher probability than full grid-dependency to operate below the maximum affordable levelized cost of electricity predicted (e.g. 231 €/MWh for a dwelling in a variable market scenario).

For a community, the robust design achieves a significant self-sufficiency ratio ($\geq 54\%$) and includes both a battery stack and a hydrogen-based energy system. This design is least-sensitive to real-life uncertainty as the decoupling of hydrogen power and hydrogen energy enables to curb the contribution of the uncertainty related to the electrolyzer and fuel cell in the levelized cost of electricity uncertainty. Moreover, these designs prove beneficial over full grid-dependency when the maximum allowed levelized cost of electricity is determined above 414 €/MWh in the fixed market conditions scenario and above 456 €/MWh in the variable market conditions scenario. Conclusively, depending on the financial flexibility of the system owner, battery and hydrogen storage

provide a higher probability to realize a levelized cost of electricity below the maximum allowed levelized cost of electricity to ensure affordability than full-grid dependency. Future work will focus on the integration of different locations. Moreover, a heat demand will be included, to fully exploit the fuel cell capability.

5. Acknowledgements

The first author acknowledges the support of Fonds de la Recherche Scientifique - FNRS [35484777 FRIA-B2].

References

- [1] F. Birol, Renewables 2018: Market analysis and forecast from 2018 to 2023, Tech. rep., International Energy Agency (2018).
- [2] M. Aneke, M. Wang, Energy storage technologies and real life applications—A state of the art review, *Applied Energy* 179 (2016) 350–377.
- [3] T. Taner, S. A. H. Naqvi, M. Ozkaymak, Techno-economic analysis of a more efficient hydrogen generation system prototype: a case study of PEM electrolyzer with Cr-C coated SS304 bipolar plates, *Fuel Cells* 19 (2019) 19–26.
- [4] T. Taner, Energy and exergy analyze of PEM fuel cell: a case study of modeling and simulations, *Energy* 143 (2018) 284–294.
- [5] D. Parra, G. S. Walker, M. Gillott, Modeling of PV generation, battery and hydrogen storage to investigate the benefits of energy storage for single dwelling, *Sustainable Cities and Society* 10 (2014) 1–10.
- [6] M. A. Pellow, C. J. Emmott, C. J. Barnhart, S. M. Benson, Hydrogen or batteries for grid storage? A net energy analysis, *Energy & Environmental Science* 8 (2015) 1938–1952.

- [7] Y. Zhang, P. E. Campana, A. Lundblad, J. Yan, Comparative study of hydrogen storage and battery storage in grid connected photovoltaic system: Storage sizing and rule-based operation, *Applied Energy* 201 (2017) 397–411.
- [8] E. L. Eriksson, E. M. A. Gray, Optimization and integration of hybrid renewable energy hydrogen fuel cell energy systems – A critical review, *Applied Energy* 202 (2017) 348–364.
- [9] G. Mavromatidis, K. Orehounig, J. Carmeliet, A review of uncertainty characterisation approaches for the optimal design of distributed energy systems, *Renewable and Sustainable Energy Reviews* 88 (2018) 258–277.
- [10] D. Bezmalinović, F. Barbir, I. Tolj, Techno-economic analysis of PEM fuel cells role in photovoltaic-based systems for the remote base stations, *International Journal of Hydrogen Energy* 38 (2013) 417–425.
- [11] A. Marrel, B. Iooss, B. Laurent, O. Roustant, Calculations of sobol indices for the gaussian process metamodel, *Reliability Engineering & System Safety* 94 (3) (2009) 742–751.
- [12] B. Sudret, Polynomial chaos expansions and stochastic finite-element methods, *Risk and Reliability in Geotechnical Engineering* Chap. 6 (2014) 265–300.
- [13] D. Coppitters, W. De Paepe, F. Contino, Surrogate-assisted robust design optimization and global sensitivity analysis of a directly coupled photovoltaic-electrolyzer system under techno-economic uncertainty, *Applied Energy* 248 (2019) 310–320.
- [14] K. Verleysen, D. Coppitters, A. Parente, W. De Paepe, F. Contino, How can power-to-ammonia be robust? Optimization of an ammonia synthesis plant powered by a wind turbine considering operational uncertainties, *Fuel* 266 (2020) 117049.

- [15] E. Kuznetsova, C. Ruiz, Y.-F. Li, E. Zio, Analysis of robust optimization for decentralized microgrid energy management under uncertainty, *International Journal of Electrical Power & Energy Systems* 64 (September 2015) (2015) 815–832.
- [16] D. E. Majewski, M. Wirtz, M. Lampe, A. Bardow, Robust multi-objective optimization for sustainable design of distributed energy supply systems, *Computers & Chemical Engineering* 102 (2017) 26–39.
- [17] K. Akbari, M. M. Nasiri, F. Jolai, S. F. Ghaderi, Optimal investment and unit sizing of distributed energy systems under uncertainty: A robust optimization approach, *Energy and Buildings* 85 (2014) 275–286.
- [18] A. Parisio, C. Del Vecchio, A. Vaccaro, A robust optimization approach to energy hub management, *International Journal of Electrical Power & Energy Systems* 42 (2012) 98–104.
- [19] M. Castañeda, A. Cano, F. Jurado, H. Sánchez, L. M. Fernández, Sizing optimization, dynamic modeling and energy management strategies of a stand-alone PV/hydrogen/battery-based hybrid system, *International Journal of Hydrogen Energy* 38 (2013) 3830–3845.
- [20] BISEPS, Update on the digital meter and grid tariffing methodology in Flanders, Tech. rep., Interreg 2 Seas Mers Zeeën - European Regional Development Fund (2018).
- [21] W. F. Holmgren, C. W. Hansen, M. A. Mikofski, pvlib python: a python package for modeling solar energy systems, *The Journal of Open Source Software* 3 (2018) 884.
- [22] J. S. Stein, W. F. Holmgren, J. Forbess, C. W. Hansen, PVLIB: Open source photovoltaic performance modeling functions for Matlab and Python, in: *2017 IEEE 44th Photovoltaic Specialist Conference, PVSC 2017*, IEEE, 2017, pp. 1–6.

- [23] W. De Soto, S. A. Klein, W. A. Beckman, Improvement and validation of a model for photovoltaic array performance, *Solar Energy* 80 (2006) 78–88.
- [24] Sunpower, X-Series residential solar panels: supplementary technical specifications.
- [25] G. de Oliveira e Silva, P. Hendrick, Lead–acid batteries coupled with photovoltaics for increased electricity self-sufficiency in households, *Applied Energy* 178 (2016) 856–867.
- [26] B. Battke, T. S. Schmidt, D. Grosspietsch, V. H. Hoffmann, A review and probabilistic model of lifecycle costs of stationary batteries in multiple applications, *Renewable and Sustainable Energy Reviews* 25 (2013) 240–250.
- [27] S. Blaifi, S. Moulahoum, I. Colak, W. Merrouche, An enhanced dynamic model of battery using genetic algorithm suitable for photovoltaic applications, *Applied Energy* 169 (2016) 888–898.
- [28] B. Zakeri, S. Syri, Electrical energy storage systems: A comparative life cycle cost analysis, *Renewable and Sustainable Energy Reviews* 42 (2015) 569–596.
- [29] R. Dufo-López, J. M. Lujano-Rojas, J. L. Bernal-Agustín, Comparison of different lead–acid battery lifetime prediction models for use in simulation of stand-alone photovoltaic systems, *Applied Energy* 115 (2014) 242–253.
- [30] C. Phurailatpam, B. S. Rajpurohit, L. Wang, Planning and optimization of autonomous DC microgrids for rural and urban applications in India, *Renewable and Sustainable Energy Reviews* 82 (2018) 194–204.
- [31] I. Pawel, The cost of storage - How to calculate the levelized cost of stored energy (LCOE) and applications to renewable energy generation, *Energy Procedia* 46 (2014) 68–77.

- [32] P. Komor, J. Glassmire, Electricity storage and renewables for island power: a guide for decision makers, Tech. rep., International Renewable Energy Agency (IRENA) (2012).
- [33] A. Buttler, H. Spliethoff, Current status of water electrolysis for energy storage, grid balancing and sector coupling via power-to-gas and power-to-liquids: A review, *Renewable and Sustainable Energy Reviews* 82 (2018) 2440–2454.
- [34] Z. Abdin, C. J. Webb, E. M. Gray, Modelling and simulation of a proton exchange membrane (PEM) electrolyser cell, *International Journal of Hydrogen Energy* 40 (2015) 13243–13257.
- [35] F. Marangio, M. Santarelli, M. Cali, Theoretical model and experimental analysis of a high pressure PEM water electrolyser for hydrogen production, *International Journal of Hydrogen Energy* 34 (3) (2009) 1143–1158.
- [36] H. Görgün, Dynamic modelling of a proton exchange membrane (PEM) electrolyzer, *International Journal of Hydrogen Energy* 31 (2006) 29–38.
- [37] K. Ameer, A. Hadjaissa, M. Ait Cheikh, A. Cheknane, N. Essounbouli, Fuzzy energy management of hybrid renewable power system with the aim to extend component lifetime, *International Journal of Energy Research* 41 (2017) 1867–1879.
- [38] K. Murugesan, V. Senniappan, Investigation of water management dynamics on the performance of a Ballard-Mark-V proton exchange membrane fuel cell stack system, *International Journal of Electrochemical Science* 8 (2013) 7885–7904.
- [39] M. Taghvaei, M. Radzi, S. Moosavain, H. Hizam, M. H. Marhaban, A current and future study on non-isolated DC–DC converters for photovoltaic applications, *Renewable and sustainable energy reviews* 17 (2013) 216–227.

- [40] G. A. Rampinelli, A. Krenzinger, F. Chenlo Romero, Mathematical models for efficiency of inverters used in grid connected photovoltaic systems, *Renewable and Sustainable Energy Reviews* 34 (2014) 578–587.
- [41] S. Wilcox, W. Marion, Users manual for TMY3 data sets, Tech. rep., National Renewable Energy Laboratory Golden, CO (2008).
- [42] Open Energy Information, Commercial and Residential Hourly Load Profiles for all TMY3 Locations in the United States, Available online: <http://en.openei.org/datasets/dataset/commercial-and-residential-hourly-load-profiles-for-all-tmy3-locations-in-the-united-states>. Accessed: 16th February 2019.
- [43] M. Montero Carrero, I. R. Sánchez, W. D. Paepe, A. Parente, F. Contino, Is There a Future for Small-Scale Cogeneration in Europe ? Economic and Policy Analysis of the Internal Humid Air Turbine Cycles, *Energies* 12 (2019) 1–27.
- [44] P. Balcombe, D. Rigby, A. Azapagic, Investigating the importance of motivations and barriers related to microgeneration uptake in the UK, *Applied Energy* 130 (2014) 403–418.
- [45] Elia, Electricity scenarios for Belgium towards 2050: Elia’s quantified study on the energy transition in 2030 and 2040, Tech. rep., Elia (2017).
- [46] S. Abraham, M. Raisee, G. Ghorbaniasl, F. Contino, C. Lacor, A robust and efficient stepwise regression method for building sparse polynomial chaos expansions, *Journal of Computational Physics* 332 (2017) 461–474.
- [47] W. De Paepe, D. Coppitters, S. Abraham, P. Tsirikoglou, G. Ghorbaniasl, F. Contino, Robust Operational Optimization of a Typical micro Gas Turbine, *Energy Procedia* 158 (2019) 5795–5803.
- [48] S. Giorgetti, D. Coppitters, F. Contino, W. D. Paepe, L. Bricteux, G. Averzano, A. Parente, Surrogate-Assisted Modeling and Robust Optimization of

a Micro Gas Turbine Plant With Carbon Capture, *Journal of Engineering for Gas Turbines and Power* 142.

- [49] P. Tsirikoglou, S. Abraham, F. Contino, Ö. Bağci, J. Vierendeels, G. Ghorbaniasl, Comparison of metaheuristics algorithms on robust design optimization of a plain-fin-tube heat exchanger, in: *18th AIAA/ISSMO Multidisciplinary Analysis and Optimization Conference*, 2017, p. 3827.
- [50] S. M. Wilcox, National solar radiation database 1991-2010 update: User's manual, Tech. rep., National Renewable Energy Lab.(NREL), Golden, CO (United States) (2012).
- [51] N. Lukač, S. Seme, K. Dežan, B. Žalik, G. Štumberger, Economic and environmental assessment of rooftops regarding suitability for photovoltaic systems installation based on remote sensing data, *Energy* 107 (2016) 854–865.
- [52] L. Reichenberg, F. Hedenus, M. Odenberger, F. Johnsson, The marginal system LCOE of variable renewables – Evaluating high penetration levels of wind and solar in Europe, *Energy* 152 (2018) 914–924.
- [53] B. Guinot, B. Champel, F. Montignac, E. Lemaire, D. Vannucci, S. Sailer, Y. Bultel, Techno-economic study of a PV-hydrogen-battery hybrid system for off-grid power supply: Impact of performances' ageing on optimal system sizing and competitiveness, *International Journal of Hydrogen Energy* 40 (2015) 623–632.
- [54] W. G. Colella, B. D. James, J. M. Moton, G. Saur, T. Ramsden, Techno-economic Analysis of PEM Electrolysis for Hydrogen Production, Tech. rep., Strategic Analysis inc. and National Renewable Energy Laboratory (NREL) (2014).
- [55] L. Placca, R. Kouta, J. F. Blachot, W. Charon, Effects of temperature uncertainty on the performance of a degrading PEM fuel cell model, *Journal of Power Sources* 194 (2009) 313–327.

- [56] T. Taner, Energy and exergy analyze of PEM fuel cell: A case study of modeling and simulations, *Energy* 143 (2018) 284–294.
- [57] S. Niaz, T. Manzoor, A. H. Pandith, Hydrogen storage: Materials, methods and perspectives, *Renewable and Sustainable Energy Reviews* 50 (2015) 457–469.
- [58] Y. Budak, Y. Devrim, Comparative study of PV/PEM fuel cell hybrid energy system based on methanol and water electrolysis, *Energy conversion and management* 179 (2019) 46–57.
- [59] E. Ozden, I. Tari, PEM fuel cell degradation effects on the performance of a stand-alone solar energy system, *International Journal of Hydrogen Energy* 42 (2017) 13217–13225.
- [60] J. Kotowicz, D. Wecel, M. Jurczyk, Analysis of component operation in power-to-gas-to-power installations, *Applied energy* 216 (2018) 45–59.
- [61] J. Wu, X. Z. Yuan, J. J. Martin, H. Wang, J. Zhang, J. Shen, S. Wu, W. Merida, A review of pem fuel cell durability: Degradation mechanisms and mitigation strategies, *Journal of Power Sources* 184 (2008) 104–119.
- [62] F. Abbasi, M. Abapour, Reliability and cost optimization of multi-input bidirectional DC/DC converter implemented in renewable sources, *Majlesi Journal of Electrical Engineering* 12 (2018) 57–65.
- [63] A. Allouhi, M. S. Buker, H. El-houari, A. Boharb, M. Benzakour Amine, T. Kousksou, A. Jamil, PV water pumping systems for domestic uses in remote areas: Sizing process, simulation and economic evaluation, *Renewable Energy* 132 (2019) 798–812.
- [64] A. Kashefi Kaviani, G. H. Riahy, S. M. Kouhsari, Optimal design of a reliable hydrogen-based stand-alone wind/PV generating system, considering component outages, *Renewable Energy* 34 (2009) 2380–2390.

- [65] M. A. Ramli, A. Hiendro, S. Twaha, Economic analysis of PV/diesel hybrid system with flywheel energy storage, *Renewable Energy* 78 (2015) 398–405.
- [66] Vlaamse Regulator van de Elektriciteits- en Gasmarkt (Flemish Regulator of the Electricity and Gas Market), Evolution of the household electricity bill, Available online: <https://infogram.com/evolutie-energiefactuur-gezin-1h7j4djlx9k94nr?live>. Accessed: 3th February 2020.
- [67] Triami Media BV, Historic inflation Belgium - CPI inflation, Available online: inflation.eu/inflation-rates/belgium/historic-inflation/cpi-inflation-belgium.aspx. Accessed: 1st August 2019 (2019).
- [68] T. H. T. Nguyen, T. Nakayama, M. Ishida, Optimal capacity design of battery and hydrogen system for the DC grid with photovoltaic power generation based on the rapid estimation of grid dependency, *International Journal of Electrical Power & Energy Systems* 89 (2017) 27–39.
- [69] A. Khiareddine, C. B. Salah, D. Rekioua, M. F. Mimouni, Sizing methodology for hybrid photovoltaic/wind/hydrogen/battery integrated to energy management strategy for pumping system, *Energy* 153 (2018) 743–762.
- [70] A. Singh, P. Baredar, B. Gupta, Techno-economic feasibility analysis of hydrogen fuel cell and solar photovoltaic hybrid renewable energy system for academic research building, *Energy Conversion and Management* 145 (2017) 398–414.

Appendix A. Additional data and figure

parameter, unit	min	max	Ref.
photovoltaic			
G , %	-9.9	+7.7	[50]
T_{amb} , K	-0.9	+0.9	[50]
power tolerance _{PV} , %	0	5	[24]
CAPEX _{PV} , €/kW _p	430	780	[51]
OPEX _{PV} , €/kW _p	16	19	[52]
hydrogen			
CAPEX _{elec} , €/kW	1400	2100	[33]
OPEX _{elec} , %	3	5	[33]
$R_{\text{c,elec}}$, %	15	20	[53, 54]
n_{elec} , kh	60	100	[33]
T_{elec} , K	347	359	[55]
p_{elec} , bar	-0.1	0.1	[56]
degradation _{elec} , $\mu\text{V}/\text{h}$	4	8	[33]
CAPEX _{tank} , €/kWh	10.4	14.4	[57]
OPEX _{tank} , %	1	2	[7, 53]
CAPEX _{FC} , €/kW	1500	2400	[58–60]
OPEX _{FC} , €/h	0.045	0.135	[58, 59]
$R_{\text{c,FC}}$, %	25	30	[58, 59]
n_{FC} , kh	20	30	[7, 26]
T_{FC} , K	347	359	[55]
p_{FC} , bar	-0.1	0.1	[56]
degradation _{FC} , $\mu\text{V}/\text{h}$	2	10	[61]
battery			
CAPEX _{bat} , €/kWh	102	354	[26]
OPEX _{bat} , €/kWh	15	28	[26, 28]

$R_{c,\text{bat}}$, €/kWh	61	141	[26, 28]
n_{bat} , cycles	500	2000	[26]
self discharge _{bat} , %/day	0.1	0.3	[28]
degradation _{bat} , %/year	3.5	4.0	[31]
converter/inverter			
CAPEX _{DCDC} , €/kW	100	200	[62, 63]
OPEX _{DCDC} , %	1	5	[64, 65]
CAPEX _{DCAC} , €/kW	342	519	[51]
OPEX _{DCAC} , %	1	5	[64, 65]
other			
E_{load} , %	+2	+7	[45]
w , €/MWh	46	97	[45]
f_w	0.2	0.4	[66]
f , %	1	3	[67]
i' , %	4	8	[68–70]

Table A.3: The ranges for the stochastic parameters, used in the Robust Design Optimization (RDO) process.

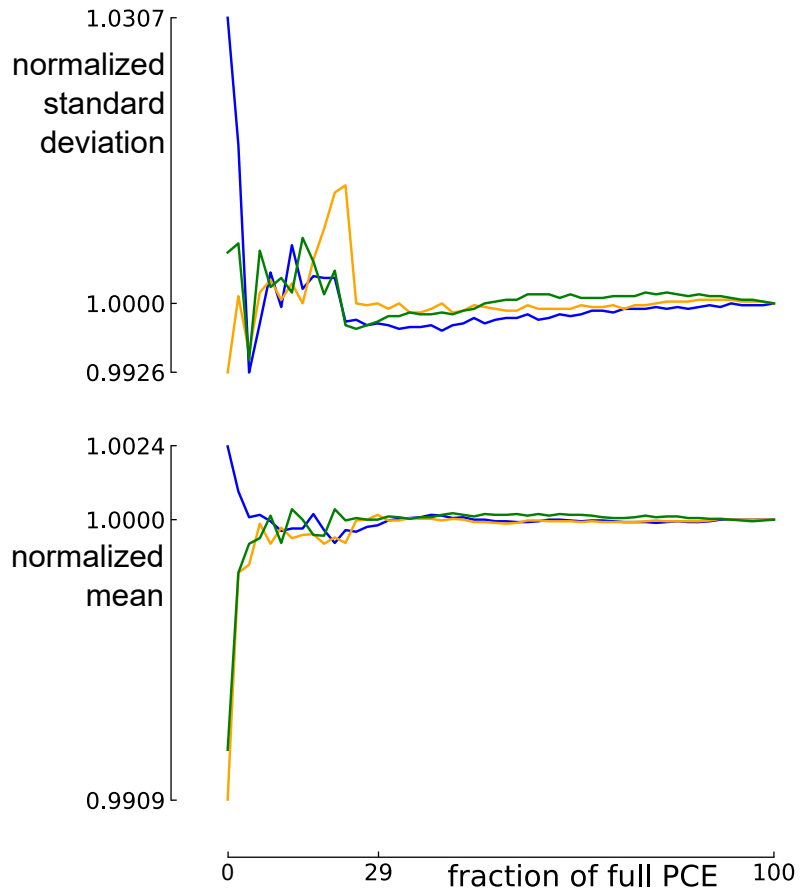


Figure A.9: The gradual increase of the initial number of real model evaluations for 3 design samples illustrates that accurate statistical moments can be acquired by evaluating only 29% of the required full PCE model evaluations.